

## Double ionization of helium in fast ion collisions: the role of momentum transfer

B Bapat<sup>†</sup>, R Moshhammer<sup>†</sup>, S Keller<sup>‡</sup>, W Schmitt<sup>†</sup>, A Cassimi<sup>§</sup>, L Adoui<sup>§</sup>,  
H Kollmus<sup>†</sup>, R Dörner<sup>||</sup>, Th Weber<sup>||</sup>, K Khayat<sup>||</sup>, R Mann<sup>¶</sup>, J P Grandin<sup>§</sup>  
and J Ullrich<sup>†</sup>

<sup>†</sup> Fakultät für Physik, Universität Freiburg, 79104 Freiburg, Germany

<sup>‡</sup> Institut für Theoretische Physik, Universität Frankfurt, 60054 Frankfurt, Germany

<sup>§</sup> Centre Interdisciplinaire Recherche avec les Ions Lourds, 14040 Caen, France

<sup>||</sup> Institut für Kernphysik, Universität Frankfurt, 60486 Frankfurt, Germany

<sup>¶</sup> Gesellschaft für Schwerionenforschung, 64291 Darmstadt, Germany

Received 23 December 1998

**Abstract.** Double ionization of helium in the perturbative regime has been explored in a kinematically complete collision experiment using 100 MeV/u C<sup>6+</sup> ions. Different ionization mechanisms are identified by inspecting the angular distribution of the electrons as a function of the momentum transfer  $q$  to the target by the projectile. For  $q < 1.2$  au, both electrons are distributed uniformly in the plane perpendicular to the projectile axis, and distinct similarities with photoionization are identified. For  $q > 1.2$  au, the faster electron resulting from a binary encounter with the projectile is emitted along the direction of momentum transfer, while the other electron is distributed uniformly. Experimental data are compared with various model calculations based on the Bethe–Born approximation with shake-off. Surprisingly, the effect of the final state interaction is found to depend decisively on the choice of the initial state wavefunction.

### 1. Introduction

Very recently, it has become possible to perform kinematically complete ion–atom collision experiments for single [1–6] and double [7] ionization. That is, the momenta of all fragments arising from the collision—the recoiling target ion and the ejected electrons—can be determined with sufficient accuracy (for a review see, e.g., [8]). This unprecedented capability permits determination of the tiny change of the projectile momentum,  $q = q_i - q_f$ , inaccessible in any direct measurement, purely from energy and momentum conservation in the reaction. The momentum transferred to the target atom is simply equal, but opposite, to the change in the momentum of the projectile. Momentum transfer in a collision is a key parameter in ion–atom collision theory. It is also known from (e, 2e) experiments—that is, kinematically complete electron impact single ionization experiments—that the direction and magnitude of the momentum transfer vector plays a crucial role in characterizing the single ionization process [9]. In this paper, we investigate the importance of this quantity for understanding double ionization reactions.

Single ionization of atoms by the impact of a fast, charged particle (of charge  $Z_p$  and velocity  $v_p$ ) is theoretically described by the first-order matrix element of a perturbation expansion in  $Z_p/v_p$ , i.e. the Bethe–Born approximation [10], which has become a benchmark theory. As first pointed out by Bethe, this matrix element for single ionization by charged

particles becomes identical to the one for ionization by a single photon, in the limit of high  $v_p$ . Moreover, depending on the magnitude of the momentum transfer ( $q$ ), charged particle impact ionization can be related to the two photonic processes leading to electron emission: photoabsorption, where the incident photon is completely absorbed, and Compton scattering, where the incident photon is inelastically scattered.

For small  $q$ , approaching the value  $\Delta E_p/v_p$  in the limit  $v_p \rightarrow c$ , where  $\Delta E_p$  is the energy loss of the projectile, the process becomes identical to the absorption of a photon of energy  $\Delta E_p$ . The emission pattern of the electron approaches a dipole distribution with respect to  $q$  (corresponding to the electric field vector in a photoabsorption event), and the electron momentum is compensated by the recoiling ion. Another aspect of this similarity was expounded by Bethe. He introduced [10] the generalized oscillator strength (GOS)—a concept related to the excitation of an electron in an atom by a harmonic electric field—to express charged particle impact ionization cross sections. The GOS has been utilized in numerous studies to characterize atomic and molecular systems, which are reviewed by Inokuti [11], and has been explored in many experiments on single ionization by electron impact [12, 13]. Wight and Van der Wiel [14], for example, measured the GOS for double and single ionization of various rare gases by electron impact at high velocities, and found excellent agreement with the GOS obtained by direct photoionization, showing the strong correspondence between the two processes. Exploring the impact of 1 GeV/u  $U^{92+}$  projectiles on helium, Moshhammer *et al* [4] recently demonstrated the equivalence of photoabsorption and ionization in collisions with fast ions. In a kinematically complete experiment, single ionization cross sections differential in the longitudinal momentum of the recoil ion and the electron, as well as cross sections differential in electron energy, were shown to closely follow those arising by exposure to an intense, ultrashort, broadband photon field. The Weizsäcker–Williams method of virtual quanta [15, 16] was used to express this analogy, though the experiment [4] was actually carried out outside the regime of formal validity of this approach ( $Z_p/v_p = 0.78$ ). More recently, analogies to photoionization in collision of 60 MeV/u  $Ar^{18+}$  ions with lithium were revealed by comparing double differential electron emission cross sections with various calculations differential in final state angular momentum of the electron, by Stolterfoht *et al* [17].

For large  $q$ , again pointed out by Bethe, the first-order matrix element for single ionization is essentially equivalent to that for Compton scattering where the incoming high-energy photon is inelastically scattered off the bound electron. Energy and momentum are balanced only by the scattered photon and the electron, the recoil ion being a mere spectator, left behind with a momentum corresponding to the Compton profile, i.e. the bound state momentum distribution, of the electron. For high-energy photons, this was demonstrated experimentally by Spielberger *et al* [18], by directly measuring the momentum of the recoil ion. Considerable effort, theoretical [19] as well as experimental [20, 21], has gone into investigating the relation between Compton scattering and ion impact ionization at large  $q$ . These investigations have been strongly motivated by total cross section measurements and the behaviour of the ratio of double-to-single ionization cross section of helium at high energies. This ratio has been found to be different in the limit of high photon or particle energies for Compton scattering, photoabsorption, and charged particle impact.

In view of this discussion, it is natural to ask whether the momentum transfer is also a key parameter in multiple ionization reactions. To answer this question, we present the results of the first kinematically complete experiment on double ionization of helium carried out in the perturbative regime ( $Z_p/v_p < \frac{1}{2}$ ). The only previous experiment of this type [4] was done in the strong coupling regime, where strong non-perturbative features were manifest in the electron spectra. In the situation considered here, however, a perturbative description of the projectile–target interaction should be perfectly appropriate. Thus, the experimental

data differential in momentum transfer are used to benchmark various first-order (Bethe–Born plus shake-off) models of double ionization. Along the lines of the above discussion, it is expected that differences should occur in double ionization dynamics for small and large momentum transfers. Indeed, we presently show that the electron angular distributions for  $q < 1.2$  au are dramatically different from those for  $q > 1.2$  au. Via the relationship  $p \sim \hbar/a$ , the small and large momentum transfer domains can be identified with distant and close collisions, respectively. This information can be used to interpret the results obtained for model calculations using different initial and final state wavefunctions.

## 2. Experiment

The experiment was performed at the Grand Accélérateur National de Ions Lourds (GANIL). Fully stripped carbon ions  $C^{6+}$  were accelerated to 100 MeV/u and focused on an internally cold supersonic jet of helium gas. The gas jet assembly is a part of the ‘reaction microscope’ which is described elsewhere in detail [22]. Briefly, it comprises a pair of parallel ceramic plates  $22 \times 20$  cm<sup>2</sup> in size, with burnt-in resistive layers on the surface, which permit the generation of a uniform electric field in any direction in the gap between the plates. The field direction can be changed as desired by controlling the voltages applied to the corners of the resistive plates. The usual configuration has the electric field antiparallel to the ion beam. A homogenous solenoidal magnetic field generated by two coils 1.5 m in diameter is also applied along the electric field direction. The overlap of the gas jet and the ion beam is arranged to be at the centre of the field-generating plates and coils. The two fields efficiently extract and guide the ions and electrons formed in the interaction volume onto large channel plate detectors on both sides of the plates. Separation of the recoil ion charge states is accomplished on the basis of the flight times, and the distances of the detectors from the interaction region are arranged to achieve a time-focusing geometry. The detectors are equipped with a delay-line readout to enable position-sensitive detection, with a resolution of approximately 200  $\mu$ m. The output from the delay lines is fed into multi-hit time-to-digital converters, capable of recording up to ten position- and time-resolved electron hits on the channel plates. In this experiment the two ejected electrons were detected as separate if their arrival times differed by more than 10 ns. Therefore, if the momentum components of the electrons in the flight direction, which are the longitudinal components in our geometry, are approximately equal, the corresponding portion of the momentum spectrum is empty. The absolute magnitude of the non-detectable difference  $|p_{e2||} - p_{e1||}|$  in the electron longitudinal momenta depends on the longitudinal momentum  $p_{e1||}$  of the electron arriving first, and is about 0.1 au for  $p_{e1||} \approx 0.5$  au and about 0.2 au for  $p_{e1||} \approx 1.0$  au. It has been verified during the analysis of the data, by intentionally increasing the dead time of the detector between two hits, that this shortcoming does not affect the distributions presented in this paper. All of these tests can be performed off-line, since the data are collected in the list mode. Knowing the flight times and the positions of arrival of the ions and electrons, combined with the accurately known and extremely homogeneous extraction fields, the trajectories of the ions and electrons are reconstructed after the experiment is over. The magnetic field in the spectrometer was about 19 G, and the electric field about 2 V cm<sup>-1</sup>. With this configuration, all electrons up to 20 eV kinetic energy are guided to the detector irrespective of the initial direction of their velocities, but electrons with higher energy ejected in the direction away from the detector are lost. In the transverse direction, all electrons with energies between 0–100 eV are accepted with an equal efficiency of about 0.6.

Performing the experiment well within the perturbative regime results in rather small ionization cross sections. For 100 MeV/u  $C^{6+}$  ions on helium, the cross section is  $1 \times 10^{-17}$  cm<sup>2</sup> for single ionization, and  $2.6 \times 10^{-20}$  cm<sup>2</sup> for double ionization. The effective areal density of

the target being  $10^{12}$  atoms  $\text{cm}^{-2}$ , one needs approximately  $10^9$  ions per second to obtain one double ionization event per second. This corresponds to a dc beam of  $7 \mu\text{A}$ , which is about the maximum current available at GANIL at this energy. In addition, since a timing signal is needed for time-of-flight measurements, and single ion counting is impossible at the rate of  $10^{10}$  Hz, it is essential to have a pulsed beam. Unique to GANIL is the ability to deliver beam bunches narrower than 1 ns at nearly any repetition rate. A bunch width of 1 ns, which was controlled by a separate ion detector, was just enough to obtain optimum momentum resolution in this experiment. The experiment was run at a pulse separation of  $7 \mu\text{s}$ , well beyond the maximum electron flight time of  $0.2 \mu\text{s}$ . In order to ensure that the two ejected electrons and the recoil ion originated from the same double ionization event, it was crucial to ensure that the single ionization probability per pulse was far below one, and a safe value of  $10^{-2}$  was chosen. Due to the flexibility in the time structure of the beam pulses, GANIL was the only place worldwide to perform this experiment. About 5000 completely determined double ionization events were recorded in less than 20 h of beam-time.

### 3. Calculations

For collision velocities much larger than the velocity of the bound electrons, and for small perturbations ( $Z_p/v_p = 0.1$  au in the present case), the first-order Born approximation can be used to describe the interaction between the projectile and the target. Since this description includes just a single projectile–target interaction, double ionization can only occur through a secondary process involving an electron–electron interaction. We therefore use a combination of the standard Bethe–Born theory for single ionization [10] with the shake-off model for double ionization. In this approach, while the first electron is assumed to be removed from the atom by a direct interaction with the projectile, the second electron subsequently relaxes into the ionic continuum. This latter process is mimicked by the overlap amplitude between the atomic initial state single particle wavefunction, and the ionic single particle continuum. Thus, any description of the initial state that takes into account the electron–electron interaction, in whatever approximate fashion, will lead to a nonvanishing double ionization probability.

For the initial state, we use two kinds of atomic wavefunctions. The first is a one-parameter Hartree–Fock  $1s^2$  function, i.e. a product of two hydrogenic  $1s$  wavefunctions. This model takes the electron–electron interaction into account only via an effective charge. Correlation effects which would make the radial and angular wavefunctions of the two electrons different from each other, are not included in this ansatz. Results obtained with this model are denoted with an  $O$ . The second type includes radial correlations, i.e. it takes into account the fact that one electron will usually be closer to the nucleus, so that the potential acting on the second electron is screened more strongly. Still, both electrons occupy  $s$  states, so that this model may be called a  $1s1s'$  configuration. Corresponding results are labelled with an  $R$ .

The final state is represented by a product of two Coulomb waves. Clearly, this wavefunction, which is denoted by  $n$ , has no correlation term. The present model has previously been used by Dal Cappello and Le Ruozzo [23] in a theoretical study of the  $(e, 3e)$  process in helium. We also use a wavefunction which approximately takes into account the final state interaction between the electrons. This wavefunction is denoted by  $c$ , and the approximation involves the renormalization of the two-electron relative Coulomb wave at zero distance [24]. Such treatment of the final state interaction destroys the normalization of the wavefunctions, so that the absolute values of the cross sections have little meaning, and the results have been normalized to a common scale. The results of the calculations are labelled by a pair  $(a, b)$  signifying the choice of initial and final state wavefunction.

#### 4. Analysis and results

For fast, charged projectiles, the component of the change of the momentum of the projectile perpendicular to the direction of propagation ( $q_{\perp}$ ) is significant, while the component along the direction of propagation ( $q_{\parallel}$ ) is very small. This is evident in the distributions of  $q_{\perp}$  and  $q_{\parallel}$  for double ionization events in this experiment (figures 1(a) and (b) respectively).

In figure 1(b), the dashed curve denotes the change in the longitudinal component of the projectile momentum, obtained from momentum balance in the reaction:

$$q_{\parallel} = -(p_{R\parallel} + p_{e1\parallel} + p_{e2\parallel}). \quad (1)$$

A FWHM of about 0.4 au is observed due to the experimental resolution of the momentum sum  $[(\Delta p_{R\parallel})^2 + (\Delta p_{e1\parallel})^2 + (\Delta p_{e2\parallel})^2]^{1/2}$ . The resolution is limited almost entirely by the uncertainty in the recoil momentum  $\Delta p_{R\parallel}$ , which is 0.3 au. The longitudinal momentum loss in a fast collision, however, can also be determined from the energy loss of the projectile  $\Delta E_p$ :

$$q_{\parallel} = \Delta E_p/v_p = -(E_R + E_{e1} + E_{e2} + U_{\text{He}}^{(2)})/v_p. \quad (2)$$

The electron energies  $E_{e1}$  and  $E_{e2}$  are measured, the double ionization potential of helium  $U_{\text{He}}^{(2)}$  is accurately known, and the recoil energy  $E_R$ , though measured, is in all cases less than 0.02 au, hence negligible (see also Schulz *et al* [25]). This experimental result, (continuous curve in figure 1(b)), has about five times better resolution than that obtained using equation (1). It also has a sharp threshold at  $q_{\parallel} = U_{\text{He}}^{(2)}/v_p$ , demonstrating that the longitudinal momentum transfer is extremely small for double ionization events.

Thus, it is the transverse component,  $q_{\perp}$ , which plays a key role in distinguishing between soft and hard collisions. Moreover, the magnitude of  $q_{\perp}$  may be taken to be equal to the full momentum transfer  $q$ , which we have assumed in the following discussion. Our analysis is based on angular distributions of the electrons in the plane transverse to the beam axis, i.e. the azimuthal plane (figure 2). The electron momentum vectors are projected onto the azimuthal plane, which by definition contains the  $q_{\perp}$  vector. We take the direction of the  $q_{\perp}$  vector as the reference direction (azimuthal angle zero), and analyse the in-plane angles between the projected vectors. The instrumental acceptance for momenta in the transverse plane is very high due to the strong confining effect of the magnetic field, hence the results are not affected by instrumental factors.

##### 4.1. General features

In order to investigate the role of momentum transfer on double ionization dynamics, domains of large and small momentum transfers have to be specified. As a reasonable approximate criterion, one might consider whether or not the momentum transferred by the projectile is enough to ionize one electron. This value of  $q$  is 1.34 au. Since we wish to make a comparison of soft collisions and photoionization, we limit  $q$  to a value smaller than this critical value. An initial analysis showed that for  $q < 0.8$  au the events were distinctly similar to photoionization, while for  $q > 1.2$  au they were very different. Had we chosen  $q = 0.8$  au as the upper bound for soft collisions, there would have been many events in the soft collision domain with relatively large, and difficult to estimate, errors in the angular distribution, owing to the limited resolution of  $q$  below about 0.5 au. Moreover, it is logical to have only one value of  $q$  demarcating soft and hard collisions, which we choose to be  $q = 1.2$  au. Shifting the demarcating value to 1.34 au does not change the angular distributions in the large momentum transfer domain significantly, but the distributions in the small momentum transfer domain do get obscured.

The errors in the abscissas (i.e. the number of events) of angular distributions are to a large extent only statistical. The major errors come about in the ordinates (i.e. the angle itself). The

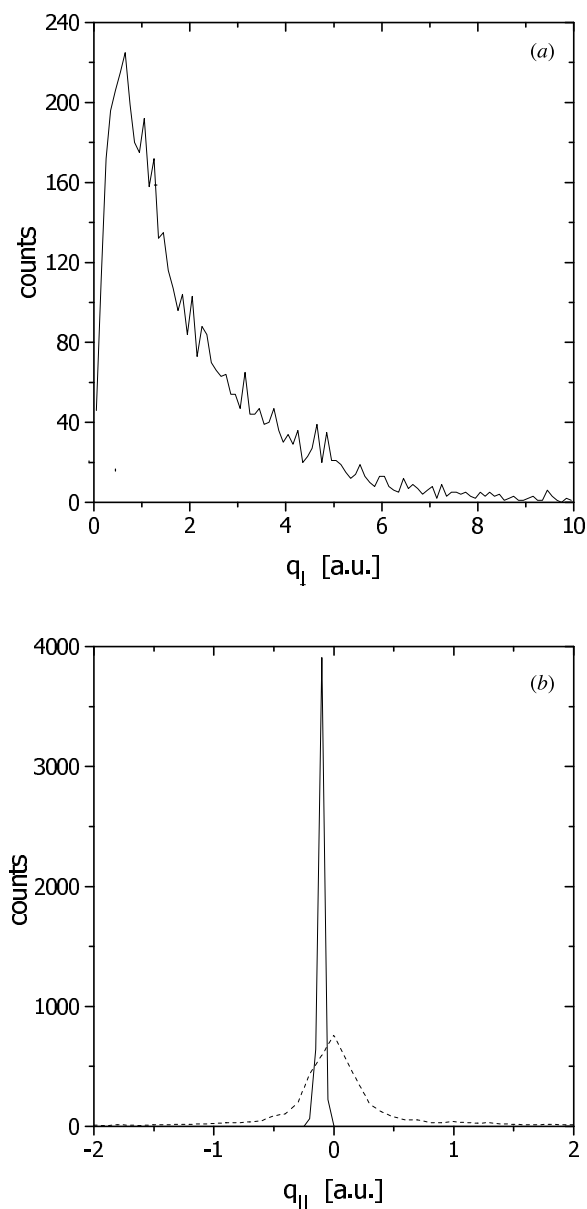


**Figure 1.** The distribution of the change of the momentum of the projectile: (a) transverse component, (b) longitudinal component. The dashed curve in (b) represents the result obtained from momentum conservation in the reaction, as given by equation (1), while the continuous curve in (b) represents the result obtained from the measured energy loss of the projectile, following equation (2).

error in determining the angles is rather difficult to estimate, because it varies from event to event, depending on the momenta of the particles. When the momentum transfers and the electron momenta are small, say  $<0.5$  au, the error in the angle could be as much as  $15^\circ$ .

Figures 3(a) and (b) show the azimuthal angular distributions for the two electrons

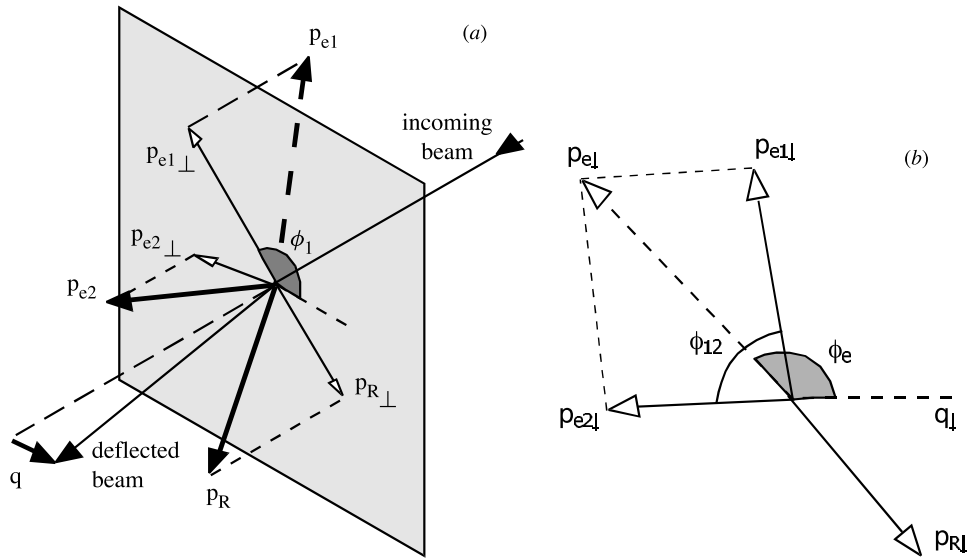


**Figure 2.** (a) The geometry of the collision. The projections of the momentum vectors of the fragments on the azimuthal plane and the momentum change of the projectile are shown. (b) The various azimuthal angles described in the text.  $\vec{p}_{e\perp}$  is the vector sum of the electron momenta:  $\vec{p}_{e1\perp} + \vec{p}_{e2\perp}$ . The figure is not to scale.

emitted in double ionization events for momentum transfers less than and greater than 1.2 au, respectively. We label the more energetic electron as electron 1, and the less energetic one as electron 2. For soft collisions, both electrons show a uniform distribution in the transverse plane, but for hard collisions, electron 1 is preferentially scattered opposite to  $q_{\perp}$ , i.e. along the momentum transfer direction. The strongly directed emission of electron 1 indicates that it is removed by a direct encounter with the projectile, while the electron 2 is removed by an indirect process, probably providing a signature of a shake-off. In contrast, for soft collisions, there are no preferred emission directions, suggesting that the emission is governed by target properties alone, and the direction of momentum transfer plays a relatively insignificant role. Apart from this strong difference in the azimuthal angular distributions of the individual electrons in the two domains, there are other differences, which we examine separately.

#### 4.2. Small momentum transfers

In the domain of small momentum transfers, the kinetic energy gained by the target electrons, due to the momentum transferred to the target, is not sufficient to overcome the binding energy. However, the fact that we nevertheless observe two free electrons, implies that there is sufficient energy transfer. This is exactly equivalent to the situation in photoionization, where there is negligibly small momentum transfer  $p_{\gamma} = E_{\gamma}/c$ , and hence it is appropriate to compare this domain with photoionization. Indeed, in this situation, the Bethe single ionization matrix element is dominated by contributions of dipole transitions [10].

The kinematics of photoionization is characterized by three main features: (i) recoil-ion momentum and sum momenta of the electrons balance each other, (ii) the sum momentum of the electrons shows a dipole pattern with respect to the polarisation vector of the photon, and (iii) electron emission in the same or opposite direction is forbidden if the electrons have equal energies. For discussion of these characteristics, see, e.g., Schmidt [26], Spielberger

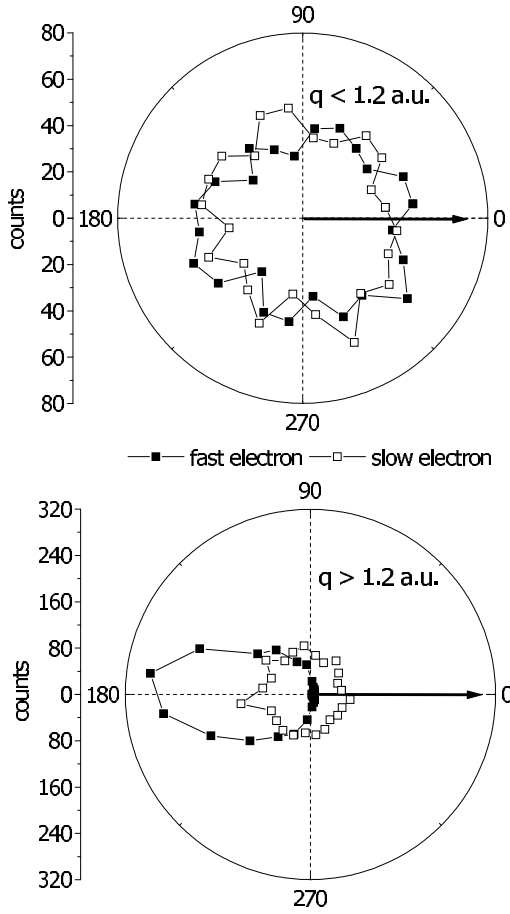


**Figure 3.** Experimental azimuthal angular distributions of the slow and fast electrons for small and large momentum transfers. The arrow represents the direction of the transverse component of the change of the projectile momentum ( $q_{\perp}$ ), which is taken to be the reference direction. The scale on the left shows the counts.

*et al* [18], and Dörner *et al* [27]. We try to look for these features in fast ion induced double ionization.

To simplify matters, we reduce the four-body events to three-body events by reducing the two electron coordinates to a single centre of mass coordinate:

$$\mathbf{p}_e = \mathbf{p}_{e1} + \mathbf{p}_{e2}. \quad (3)$$

The remaining coordinate is simply the difference vector of the two electron momenta:

$$\mathbf{p}_{12} = \mathbf{p}_{e2} - \mathbf{p}_{e1}. \quad (4)$$

When  $q$  is small, the momentum conservation condition  $\mathbf{p}_e + \mathbf{p}_R + \mathbf{q} = 0$  implies that the vectors  $\mathbf{p}_e$  and  $\mathbf{p}_R$  should be approximately of equal length, and at  $180^\circ$  to each other. Thus, the first feature of photoionization is trivially recovered here.

The second feature, concerning the dipole emission pattern of the  $\mathbf{p}_e$  vector, is displayed in figure 4(a). The dipole distribution is usually written in the form

$$\frac{d^2\sigma}{d\chi dE} = \frac{d\sigma}{dE} [1 + \beta(E)P_2(\cos \chi)], \quad (5)$$

where  $P_2$  is the second-order Legendre polynomial;  $\chi$  is the angle between the sum vector of the electron momenta and the electric field axis of the photon;  $E$  is the sum of the electron energies,  $\beta$  is the asymmetry parameter. In order to compare with photoionization, one has to

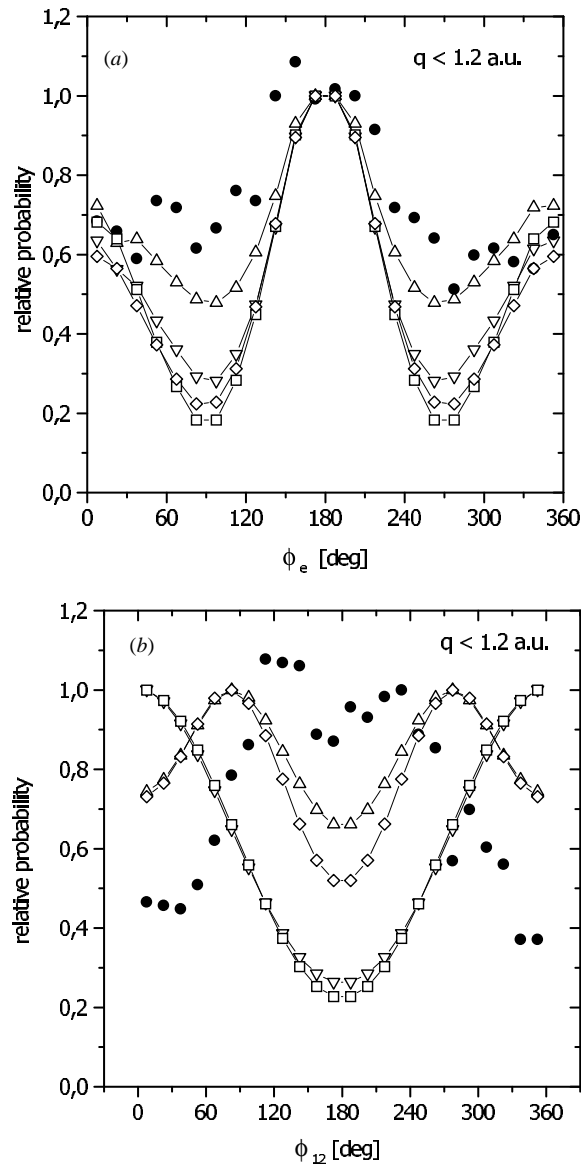


**Figure 4.** Angular distribution in the azimuthal plane for soft collisions,  $q < 1.2$  au. (a) The distribution of the sum-vector of the transverse components of the electron momenta, (b) the distribution of the azimuthal angle between the momentum vectors of the two electrons: ● experiment,  $\Delta$  ( $O, c$ ) calculations,  $\nabla$  ( $O, n$ ) calculations,  $\diamond$  ( $R, c$ ) calculations,  $\square$  ( $R, n$ ) calculations.

specify the direction of the ion induced electric field, which is mainly transverse to the beam direction, and along the direction of  $q_\perp$ , in the azimuthal plane [4]. Hence, in the present case, the azimuthal angle  $\phi_e$ , measured with respect to the direction of  $q_\perp$  (see figure 2(b)), is analogous to the angle  $\chi$  of equation (5).

Our distribution does not show a pronounced dipole pattern: a weak peak is observed in the direction of momentum transfer ( $\phi_e \simeq 180^\circ$ ), but the intensity in the direction of the projectile

deflection ( $\phi_e \simeq 0^\circ, 360^\circ$ ), is also large—about two-thirds the intensity along the direction of momentum transfer. The calculations predict a more dipole-like distribution, irrespective of the choice of the initial or final state wavefunctions, with a pronounced maximum at  $\phi_e = 180^\circ$ , the latter feature being in good agreement with experimental results. This dipole-like pattern is washed out if the final state interaction between the electrons is included into the model with an uncorrelated  $1s^2$  initial state wavefunction, bringing the calculated values in good agreement with experiment (the  $(O, c)$  results). Evidently, if one takes a radially correlated initial state, in which the two electrons are at different distances from the nucleus, the choice of the final state wavefunction does not have a large influence on the angular distribution (the  $(R, n)$  and  $(R, c)$  results). These calculations make it clear that the separation of the omnipresent electron–electron interaction into ‘initial state correlation’ and ‘final state correlation’ is artificial, as the effect of final state interaction depends on the choice of the initial state wavefunction. Thus, a very important finding of our work is that both are equally important in describing the experimental data, and the frequently made statements that one is more important than the other for two-electron processes, are on weak grounds.

One expects from the theory and from the photoelectron spectra that, for small momentum transfers, we should observe a dipole pattern for the electron sum momentum. The reasons for not observing it could be as follows. None of the initial state wavefunctions used in the calculations includes angular electron–electron correlation, to which the experimental data may be sensitive. Moreover, the momentum transferred, though less than 1.2 au, is still significantly larger than in photoionization, and the directions of the momentum transfer in the two cases are orthogonal to each other. These features show up as a peak along the momentum transfer direction in the electron sum momentum distributions, which will not be observed in a  $(\gamma, 2e)$  process. Depending on the photon energy, and the partition of the excess energy between the ejected electrons, the dipole pattern in a  $(\gamma, 2e)$  experiment is often weak, especially near the threshold [3, 27]. In order to make a more quantitative comparison with photoionization, it is tempting to reduce the upper limit of the momentum transfer for soft collisions. However, this is not possible in the present case, since the momentum resolution for  $q$ , which is determined by the sum of the uncertainties in the measured momenta of the recoils and the electrons, is not better than 0.5 au. For momentum transfers close to this value, the direction of the  $q_\perp$  vector itself is uncertain, so that any distribution measured with respect to  $q_\perp$  is not meaningful for very small values of  $q$ .

The third feature of photo-double ionization, that equal energy electrons may not be emitted in the same or opposite directions, is examined in our data in a restricted sense, by plotting the interelectron angle  $\phi_{12}$ , integrated over all energy distributions and energy partitions (see figure 4(b)). This corresponds to simultaneous measurement of photoelectrons at different photon energies, with all possible energy sharings, which has been performed by Dörner *et al* [27]. At photon energies 1 eV and 20 eV above threshold, the most probable interelectron angle is found to be  $125^\circ$ , with a strongly reduced probability for electron emission in the same direction and a less pronounced minimum for electron emission in opposite directions. This feature is clearly seen in figure 4(b), where we see a dip in the distribution of events at  $180^\circ$ , broad maxima around  $130^\circ$  and  $230^\circ$  and reduced intensity of emission in the same direction ( $\phi_{12} < 60^\circ$  or  $\phi_{12} > 300^\circ$ ).

In figure 4(b), the comparison of the experimental data with various calculations shows a qualitative agreement, even with the  $(O, c)$  model, which gave much better agreement with the data than other models, for the distribution of the electron sum momenta. Different from the experimental data, and different from the results of photoionization, the calculated maxima are found near  $90^\circ$  and  $270^\circ$ , and the minimum for emission in opposite directions is more pronounced than the experimental minimum, while the observed intensity for emission in the

same direction is much lower than the calculated value. Comparison with calculations  $(O, n)$ , using wavefunctions without the final state interaction again emphasize the importance of this interaction. However, in the light of the discussion about the distribution of the electron sum momenta, it is unclear whether the difference between the results of various calculations is due to the missing initial state correlation or due to an underestimated influence of the final state interaction. We feel this is a crucial question, which should be clarified using improved wavefunctions.

#### 4.3. Large momentum transfers

For events with large momentum transfers, the most significant change is seen in the emission pattern of the fast electron (figure 3). In sharp contrast to the small momentum transfer case, here the fast electron is emitted preferentially along the direction of the momentum transfer, compensating most of the momentum lost by the projectile. The slow electron, on the other hand, exhibits an isotropic distribution. Thus, the more energetic electron strongly determines the sum momentum of the two electrons, which, as a consequence, is sharply peaked along the momentum transfer direction, unlike the case in soft collisions. This behaviour is seen in figure 5(a), which is in significant contrast to the case of soft collisions. Also plotted are different theoretical predictions, which are all in good agreement with the experiment. Due to the very different energies of the two outgoing electrons, the choice of neither the initial state, nor the final states is decisive although, again, the agreement with the  $(O, c)$  model is the best. The reason for this insensitivity could be as follows. A hard, direct projectile–electron encounter is a binary process, where the other electron and the nucleus are merely spectators, so that the initial state correlation is unimportant in determining the final state of this electron. The interaction between the two outgoing electrons would also be negligible in this case, since the energetic electron is removed rapidly from the target.

This is not the case for the relative emission angle between the two electrons, as seen from figure 5(b). In contrast to the situation for small momentum transfers, the experimental distribution of the interelectron angle for hard collisions is quite flat near  $180^\circ$  and shows a gradual dip away from  $180^\circ$ . Calculations neglecting the final state interaction predict exactly the opposite behaviour: that both electrons should be ejected in the same direction. This has been pointed out to be an artefact of the method by its authors [23]. Including the final state interaction with uncorrelated initial states again brings about a remarkable agreement with the experimental data (the  $(O, c)$  model). Now, however, in contrast to the soft collision case, the model including the radial correlation in the initial state is also sensitive to the inclusion of final state interaction, bringing the  $(R, c)$  calculations in close agreement with the experimental data. Thus, one observes again that the effect of inclusion of the final state interaction depends on the choice of the initial state, though the effect is not as dramatic as in the case of soft collisions.

The reasons for this are clear: first, the final state interaction is less important due to the unequal energy sharing between the electrons. Second, due to the direct momentum transfer to one of the electrons by the projectile, the removal of the second electron is expected to be less sensitive to the details of the initial state correlation. In the small momentum transfer (photoabsorption-like) domain, double ionization may be viewed as dissociation of the charges in the neutral He atom. Along the lines of the discussion in [3], the He atom may be thought of as a dipole with the nucleus as the positive pole and the electron pair as the negative pole. If double ionization were to be looked at as dissociation of this dipole, then only correlated initial state wavefunctions exhibiting a large dipole moment would contribute significantly to the double ionization amplitude. On the other hand, since Compton scattering dominates

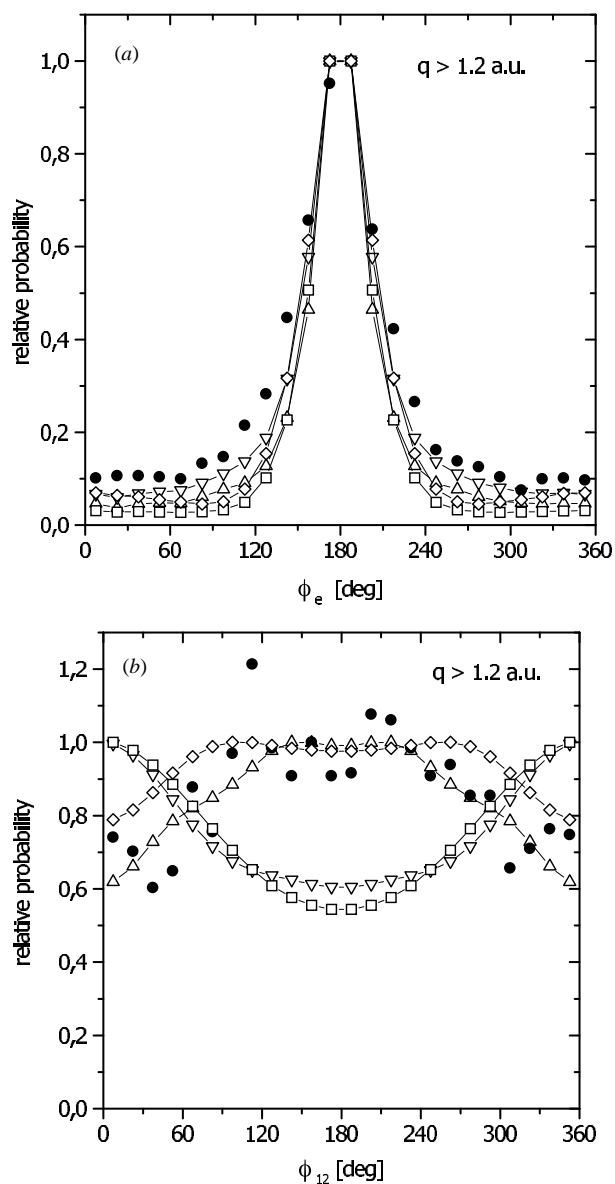


**Figure 5.** Angular distribution in the azimuthal plane for hard collisions,  $q > 1.2$  a.u. (a) The distribution of the sum vector of the transverse components of the electron momenta, (b) the distribution of the azimuthal angle between the momentum vectors of the two electrons: ● experiment,  $\Delta$  ( $O, c$ ) calculations,  $\nabla$  ( $O, n$ ) calculations,  $\diamond$  ( $R, c$ ) calculations,  $\square$  ( $R, n$ ) calculations.

over photoabsorption at large photon energies, i.e. at smaller photon wavelengths, Compton scattering is expected to sample those parts of the wavefunction in which the two electrons are uniformly distributed around the nucleus. Thus, large and small momentum transfer reactions are expected to probe different aspects of the initial state wavefunctions.

## 5. Conclusions

In summary, we have performed a kinematically complete experiment on double ionization of helium by ion impact in the domain of small perturbations, where the theoretical treatment is not too complicated and can be modelled by a combination of the Born–Bethe approximation for single ionization with the shake-off model for the removal of the second electron. The analysis presented here shows a clear division of double ionization events into hard and soft collisions, or equivalently, near and distant encounters of the projectile with the helium target. As a demarcating value for small and large momentum transfers, the average value of the momentum of the bound electron has been shown to be a reasonable choice. Significant differences between the angular distributions of the two ejected electrons are observed in the two domains.

In soft collisions leading to double ionization, distinct similarities with photoionization have been brought out. Hard collisions can be thought of as a two-step process: the direct removal of one electron, followed by removal of the other due to an indirect interaction. In both regimes, the interelectron angles and the electron sum momentum distributions are consistent with this picture of the collision.

The simple model calculation presented agrees with the experiment in both domains of momentum transfer, if the final state interaction between the electrons is accounted for. Performing model calculations with or without the radial correlation in the initial state, combined with the inclusion or exclusion of the final state electron–electron correlation, leads to surprising insight into the role of both correlations and, more importantly, into their opposing influence on the electron angular distributions.

Thus, one central finding of this work is that the choice of the initial state wavefunction decisively determines to what extent the so-called final state interaction influences the experimental outcome. One is then led to say that the distinction between the initial state interaction and the final state interaction is rather artificial. The result, that the uncorrelated  $1s^2$  wavefunction gave better agreement with the observed angular distributions, is very surprising at first glance. Even though the radially correlated wavefunctions give better estimates of the binding energy, they are worse than the  $1s^2$  wavefunctions for the representation of the spatial characteristics of the initial state.

It would be extremely interesting to use more realistic bound state wavefunctions which include electron–electron angular correlations, and find out to how much more information—beyond the total energy—they are capable of delivering. Experiments with increased statistical significance of the data are essential to obtain fully differential cross sections [28], so that a complete comparison with theory may be made.

## Acknowledgments

We are grateful to the GANIL for providing an excellent beam, the CIRIL group for their hospitality, and their engineers and technicians for continuous help in setting up the experiment and assistance during and after the beam time. Special gratitude goes to the technician responsible for the beam suppressor and the optimization and control of beam pulsing during the whole run. We gratefully acknowledge financial support from the GSI, as well as from the European Community under the programme ‘Access to large facilities’, and from the Sonderforschungsbereich-276 project ‘Low-energy electrons in the continuum of nuclei’.

## References

- [1] Moshhammer R, Ullrich J, Unverzagt M, Schmitt W, Jardin P, Olson R E, Mann R, Dörner R, Mergel V and Buck U 1994 *Phys. Rev. Lett.* **73** 3371
- [2] Mergel V et al 1995 *Phys. Rev. Lett.* **74** 2200
- [3] Dörner R et al 1996 *Phys. Rev. Lett.* **77** 1024
- [4] Moshhammer R et al 1997 *Phys. Rev. Lett.* **79** 3621
- [5] Abdallah M A, Wolff W, Wolf H E, Cocke C L and Stöckli 1998 *Phys. Rev. A* **58** R3379
- [6] Moshhammer R, Ullrich J, Kollmus H, Schmitt W, Unverzagt M, Schmidt-Böcking H, Wood C J and Olson R E 1997 *Phys. Rev. A* **56** 1351
- [7] Moshhammer R, Ullrich J, Kollmus H, Schmitt W, Unverzagt M, Jagutzki O, Mergel V, Schmidt-Böcking, Mann R, Wood C J and Olson R E 1996 *Phys. Rev. Lett.* **77** 1242
- [8] Ullrich J, Moshhammer R, Dörner R, Jagutzki O, Mergel V, Schmidt-Böcking and L Spielberger 1997 *J. Phys. B: At. Mol. Opt. Phys.* **30** 2917
- [9] Lahmam-Benani A 1991 *J. Phys. B: At. Mol. Opt. Phys.* **24** 2401
- [10] Bethe H A 1930 *Ann. Phys., Lpz.* **5** 325
- [11] Inokuti M 1971 *Rev. Mod. Phys.* **43** 297
- [12] Backx C, Tol R R, Wight G R and Van der Wiel M J 1975 *J. Phys. B: At. Mol. Phys.* **8** 2050
- [13] Van der Wiel M J and Wiebes G 1971 *Physica* **53** 225
- [14] Wight G R and Van der Wiel M J 1976 *J. Phys. B: At. Mol. Phys.* **9** 1319
- [15] von Weizsäcker C F 1934 *Z. Phys.* **88** 612
- [16] Williams E J 1934 *Phys. Rev.* **45** 729
- [17] Stolterfoht N et al 1998 *Phys. Rev. Lett.* **80** 4649
- [18] Spielberger L et al 1995 *Phys. Rev. Lett.* **74** 4615
- [19] Wang J, McGuire J H and Burgdörfer J 1995 *Phys. Rev. A* **51** 4687
- [20] Levin J C, Sellin I A, Johnson B M, Lindle D W, Miller R D, Berrah, Azuma Y, Berry H G and Lee D H 1993 *Phys. Rev. A* **47** R16
- [21] Samson J A R, Greene C H and Bartlett R J 1993 *Phys. Rev. Lett.* **71** 201
- [22] Moshhammer R, Unverzagt M, Schmitt W, Ullrich J and Schmidt-Böcking H 1996 *Nucl. Instrum. Methods B* **108** 425
- [23] Dal Capello C and Le Ruozo H *Phys. Rev. A* **43** 1395
- [24] Garibotti C R and Miraglia J E *Phys. Rev. A* **21** 572
- [25] Schulz M, Moshhammer R, Schmitt W, Kollmus H, Mann R, Hagmann S, Olson R E and Ullrich J 1998 *Phys. Rev. Lett.* submitted
- [26] Schmidt V 1997 *Electron Spectrometry of Atoms using Synchrotron Radiation (Cambridge Monographs on Atomic, Molecular and Chemical Physics)* (Cambridge: Cambridge University Press) section 1.4
- [27] Dörner R et al 1998 *Phys. Rev. A* **57** 1074
- [28] Dorn A, Moshhammer R, Schröter C D, Zourous T J M, Schmitt W, Kollmus H, Mann R and Ullrich J 1998 *Phys. Rev. Lett.* **82** 2496